Evaluation of Flexible Rogowski Coil Performances In Power Frequency Applications

Evaluation of Flexible Rogowski Coil Performances in Power Frequency Applications

Mario Chiampi, Gabriella Crotti, and Andrea Morando

***Abstract*—This paper investigates the effects of some influence quantities on the measurement of power frequency sinusoidal currents by means of flexible Rogowski coil sensors. The analysis is carried out through a numerical model, which is specifically developed and allows both the prediction of the circuital and coil parameter effects and the improvement of the coil design. The estimate of the measurement uncertainty associated with the on-site use of a flexible and openable Rogowski coil is finally given by assuming relatively controlled operating conditions.**

***Index Terms*—Current measurement, measurement errors, modeling, Rogowski coil (RC), uncertainty.**

I. Introduction

THE ROGOWSKI COIL (RC) is a current transducer often used in electrical power applications to measure low-frequency sinusoidal and transient high currents. The basic properties of this device (linearity, wide bandwidth, galvanic isolation, lightness, and low cost) make it a good alternative to conventional current transducers, such as current transformers (CT) and shunts, and explain a large number of further applications, which include energy management, protection systems, CT calibration, current sharing, resistance welding process, and measurement of partial discharges and earth resistance of transmission towers [1]–[6]. The measurement uncertainty of RCs can significantly vary as a function of the coil characteristics and measurement conditions, ranging from some parts in 10^4 to some percent.

As known, the RC is a mutual inductor, whose mutual inductance can be easily estimated on the basis of its geometry [3] under the assumption of the following ideal conditions:

- circular coil shape;
- power conductor of infinite length and thin cross-section;
- power conductor placed in the coil center;
- power conductor orthogonal to the coil plane;
- closed coil with turns uniformly distributed along the circumference;
- absence of any external magnetic field.

These conditions, which can be easily reproduced in a laboratory, are seldom met when commercial coils are used during on-site measurements. As a consequence, a variation of the mutual inductance coefficient can arise as a function of the coil construction characteristics and operating conditions. It becomes important then to investigate the parameters that can affect the measurement results and to predict the accuracy decrease with respect to the reference conditions. The improvement of the RC behavior and the determination of the influence quantity effects, such as the presence of an external field source, the position and path of the current-carrying conductor, and the noncircular coil shape, are often performed experimentally [6]–[12]. As an alternative, with reference to RCs for use at power frequency, some modeling approaches have been developed [13]–[16]. In particular, the influence of the straight power conductor position and the effect of the turn number are investigated in [14]. The presence of a coil terminal gap is taken into account in [15], together with the position of the power conductor. The effect of the non-orthogonal condition between the power conductor and the coil plane is described in [17], but for a current sensor with a magnetic core.

This paper describes a numerical tool, which is derived from a previous model [18], and its application to the analysis of the different behavior of RCs under non-ideal measurement conditions. The proposed model is able to simulate most of the possible RC non-idealities, together with the actual power circuit conditions. It further allows the evaluation of the combined effect of several non-idealities, which occur simultaneously. The approach developed is fast enough to be included in a Monte Carlo procedure for the estimation of the uncertainty associated with the coil use.

Attention is focused on openable and flexible Rogowski coils, which are widely used because of their ease of installation despite their lower accuracy and higher temperature sensitivity compared to both the rigid ones and those based on printed circuit boards [19]. The study is developed under sinusoidal steady-state condition at power frequency by modifying both the circuital and coil parameters, particularly the power conductor position, shape, and path; the presence of an external current; the uniformity of the turn distribution along the coil; and the noncircular coil shape. The modeling tool, validated through experimental measurements, also permits the evaluation of those design actions that improve RC behavior and its accuracy. Two of these design actions are the addition of a compensation turn or a counter-wound second winding.

Taking into account the high number of parameters that can affect the measurement accuracy, their combined effect is conveniently evaluated by a statistical procedure. Two ranges

of parameter variations are considered to simulate the on-site operating conditions. In both cases, an estimate of the measurement uncertainty is given.

II. Modeling Approach

The RC is essentially a linear mutual inductor linked with the magnetic field generated by the current $i(t)$, which flows in the power conductor (primary conductor). The electromotive force $e(t)$ induced in the coil is given by

$$e(t) = M\frac{di(t)}{dt} \tag{1}$$

where M is the mutual inductance coefficient between the coil and the primary conductor.

Under the assumption of an ideal closed coil wound with a continuous turn distribution (infinite number of turns) with a small cross-sectional area and under no-load electrical operating conditions, the mutual inductance is a constant term. Then, according to Ampere's law, the linked magnetic flux does not depend on the shape and position of the infinite length primary conductor. Whenever one of the previously mentioned conditions does not occur, a variation of the mutual inductance coefficient arises.

The developed RC model, based on a 3-D quasi-analytical formulation, provides the magnetic flux linking the coil, the mutual inductance coefficient (coil sensitivity), and the electromotive force induced at the transducer terminals. Under the assumption of a coil connected to an impedance of very high value, the current that flows in the winding is negligible since the presence of displacement currents can be disregarded under low frequency supply. The RC is considered in an open-boundary homogeneous domain. According to these hypotheses, the current $i(t)$, which flows in the filamentary primary conductor, produces in a given point *P* at the time t the magnetic vector potential expressed by the well-known relationship

$$\vec{A}\,(P,t) = \frac{\mu_0}{4\pi}\int_L \frac{i(t)d\,\vec{\ell}}{\rho_P} \tag{2}$$

where the propagation terms are neglected, μ_0 is the vacuum magnetic permeability, L is the total primary conductor length, and ρ_{P} is the distance between a point of the field source and point *P*. The magnetic flux is then given by the line integral of the potential along the winding profile Γ, that is

$$\Lambda = \int_\Gamma \vec{A}\,(P,t)\cdot d\vec{\gamma} \tag{3}$$

thanks to the divergence-free property of the magnetic flux density and to the Stokes' theorem. Integrals (2) and (3) are numerically solved by dividing the primary conductor and the coil turns into elements, whose number has been chosen on the basis of preliminary computations [18].

Since the input and output terminals of an opening coil are usually not coincident, the gap between them is quantified by an opening angle β. In the more general case of an elliptical coil, each point *P*, which belongs to the toroidal helix made of N turns, is defined by the coordinates (Fig. 1)

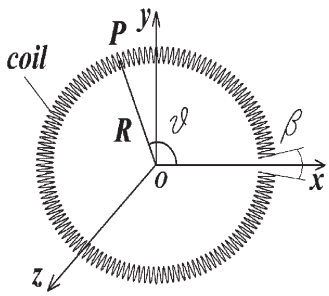

Fig. 1. Coordinate system assumed in modeling the RC.

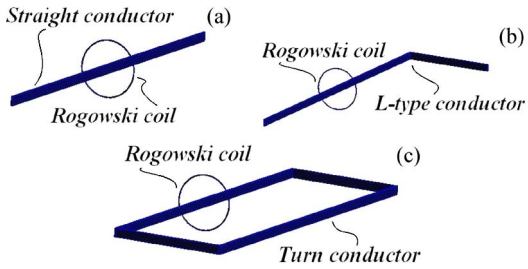

Fig. 2. Simulated power circuit paths: (a) straight; (b) L-type; and (c) turn conductors.

$$\begin{cases} x = [r\cdot\cos\gamma + S_{\max}]\cdot\cos\theta \\ y = [r\cdot\cos\gamma + S_{\min}]\cdot\sin\theta \\ z = r\cdot\sin\gamma \end{cases} \tag{4}$$

where r is the turn radius; γ is the turn angle in the plane Rz $(0 \le \gamma \le 2\pi N)$; θ is the angle in the plane xy, whose value is $(((2\pi-\beta)/2\pi N)\gamma + (\beta/2))$; and $S_{\max}$ and $S_{\min}$ are the maximum and minimum semiaxis, respectively. An RC with a circular shape can be described by imposing $S_{\max} = S_{\min} = R$, where R is the mean radius. In the following computations, the gap β is always centered at $x = S_{\max}$, $y = 0$, $z = 0$ as shown in Fig. 1.

A pitch weight vector is used to describe a non-uniform turn distribution. The element w_i of the vector is associated with the pitch of the ith turn: according to its value, the turn pitch can be enlarged $(w_i > 1)$ or reduced $(w_i < 1)$ with the constraint $\sum_{i=1}^{N} w_i = N$.

The relation (4) can be generalized to the description of RCs fitted by a compensation turn or a counter-wound compensation winding.

The model simulates the effects of bulk primary conductors with different cross-section shapes (circular and rectangular) by representing them with suitable distributions of filamentary wires. The skin effect can be taken into account by assigning proper current values to the wires.

The path of the power circuit is handled by dividing it into straight or curvilinear segments to reproduce any configuration, as for example, straight [Fig. 2(a)], L-type [Fig. 2(b)], or turn [Fig. 2(c)] conductors.

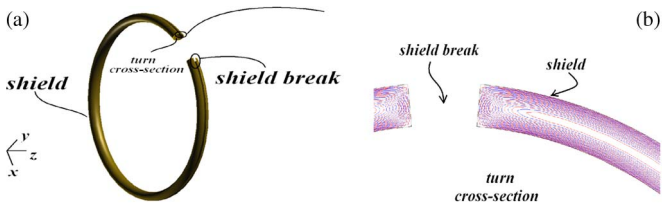

Fig. 3. (a) Sketch of the open shield geometry. (b) Current density lines induced in an open shield surrounding the turn cross-section.

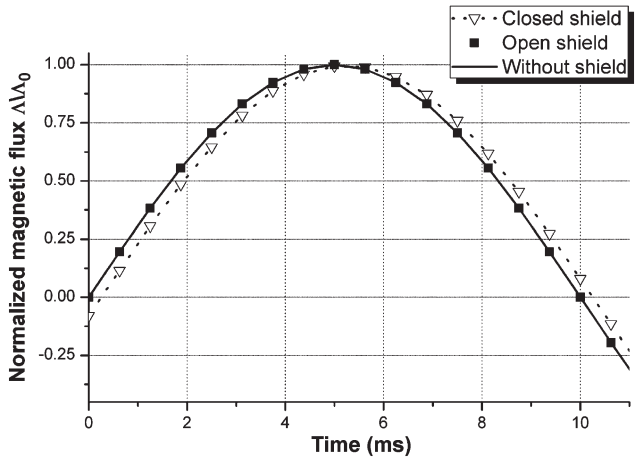

Fig. 4. Normalized magnetic flux through the turn cross-section, with closed shield, open shield, and without shield.

The modeling analysis allows the prediction of the RC behavior as a function of the following power circuit parameters:

- position of the primary conductor with respect to the coil center;
- shape of the primary conductor cross-section;
- path of the power circuit;
- tilt angle α of the primary conductor with respect to the coil plane.

Moreover, the following coil parameters can be set:

- opening angle β;
- coil eccentricity;
- non-uniform distribution of the turns along the coil;
- presence of a compensation turn or a counter-wound winding.

Actual Rogowski coils are generally shielded by an open metallic screen [2], [20], whose induced eddy currents could modify the magnetic field distribution. The evaluation of this perturbation is obtained through a finite element model based on a 2-D flux-driven T-Ω formulation [21], which provides the induced current density in the shield (Fig. 3). The computations are carried out in the Rz plane by imposing a sinusoidal magnetic flux through the turn cross-section. The shield is modeled as a hollow toroid of circular cross-section ($r = 3.6$ mm), with 1 mm thickness and $30 \cdot 10^6$ S/m electrical conductivity (aluminum shield), as shown in Fig. 3. Fig. 4 shows the time behavior of the magnetic flux through the turn cross-section, computed with a closed shield, an open shield (shield break $= 10^\circ$), and without the shield. The flux values Λ are normalized to the flux peak value without the shield Λ_0. An amplitude variation of 0.3% with a phase shift of about 4° is detected in the presence of a closed shield with respect to the unperturbed behavior. When the shield is open, the magnetic flux variation lowers to a few parts in 10^5. As a result of this analysis, the presence of the open shield is disregarded, and (2) and (3) can then be used.

TABLE I
RC AND CONDUCTOR DIMENSIONS

Primary conductor diameter	18 mm
Primary conductor length	1800 mm
Bar conductor dimensions	10 mm x 40 mm
RC mean diameter	245 mm

Fig. 5. Plexiglass disc support for the RC and circular primary conductor.

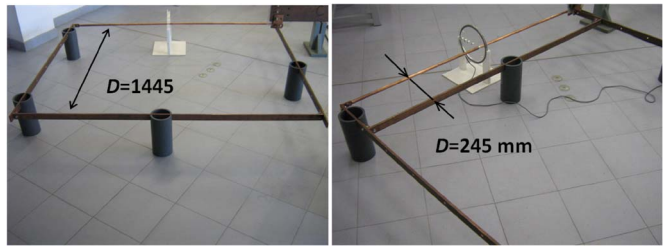

Fig. 6. RC arrangement with respect to the primary and return conductors.

III. EXPERIMENTAL VALIDATION

The validation of the model is carried out by comparing computational and measurement results under sinusoidal supply at power frequency. The investigation is performed on a commercial flexible Rogowski coil in the high-current laboratory of the Istituto Nazionale di Ricerca Metrologica of Torino.

The dimensions of the RC and the power conductors are given in Table I. To ensure good positioning accuracy, a plexiglass disc is used to support the RC and hold the primary conductor in the stated positions (Fig. 5).

The current return is made with bar conductors, whose distance D from the primary conductor can be changed (Fig. 6).

The RC mutual inductance M is evaluated as the ratio of the linked flux to the current value. The current is measured by a reference CT and the flux is obtained through the integration of the voltage induced across the RC performed by the associated integrator. A Y-bar system (Fig. 7), usually employed when performing calibrations, allows the minimization of stray magnetic fields and the symmetric positioning of the supply, the reference CT, and the device arrangement.

The scheme of the experimental setup is shown in Fig. 8.

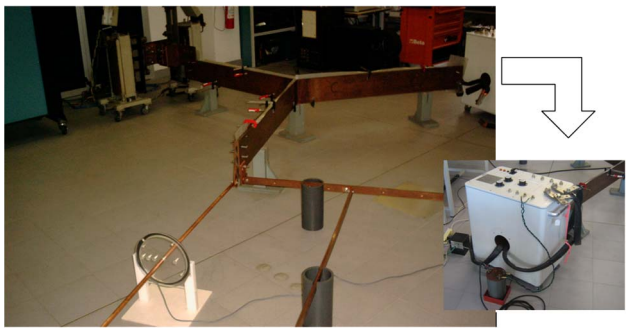

Fig. 7. Y-bar system, reference current transformer, and RC arrangement.

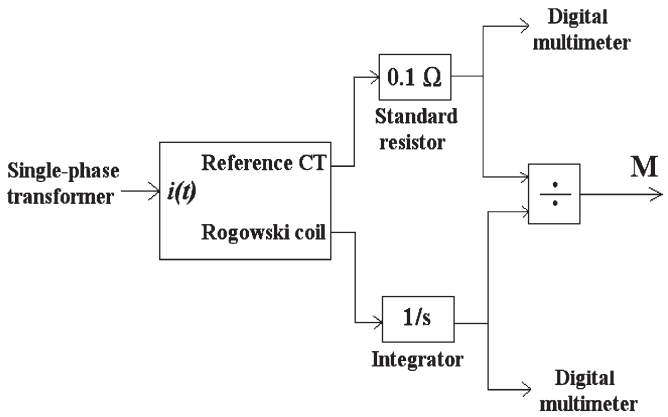

Fig. 8. Scheme of the experimental setup.

The computed and measurement results are expressed in terms of the mutual inductance M normalized to the value M_0 obtained under reference conditions, that is, when the primary conductor is centered, its axis is orthogonal to the coil plane, and the return conductor is far from the device ($D \geq 1445$ mm). It must be emphasized that M_0 does not refer to the ideal conditions, which imply an infinite primary conductor and can be well approximated when the conductor total length overcomes $\sim 50 \cdot R$.

The integrator associated with the coil is calibrated by applying reference sinusoidal voltages to verify its linearity and stability. From the results obtained, a standard uncertainty contribution of $2.5 \cdot 10^{-4}$ is attributed to the integrator. The uncertainty associated with the M/M_0 measurement values ($7 \cdot 10^{-4}$, confidence level 95%) is estimated by considering, besides the contribution of the integrator, that due to the coil positioning on the support.

Since the turn number of the commercial RC is not accurately known, some computations are performed by increasing N from 130 to 3 000. The results show that N does not appreciably affect the value of M/M_0, provided that all the other coil parameters are unvaried. Thus, a coil with 130 turns is used to reduce the computational time. Table II summarizes the main features of the model used to simulate the Rogowski coil.

Figs. 9 and 10 compare measurements and computations when the position of the primary and return conductors are varied, respectively.

In Fig. 9, the primary conductor is moved along the x-axis (Fig. 5) and the return conductor is kept 1 445 mm away from

TABLE II
MODEL PARAMETERS

RC mean radius R	122.5 mm
RC turn cross-section diameter	7 mm
Number of turns, N	130
Primary conductor length	1800 mm

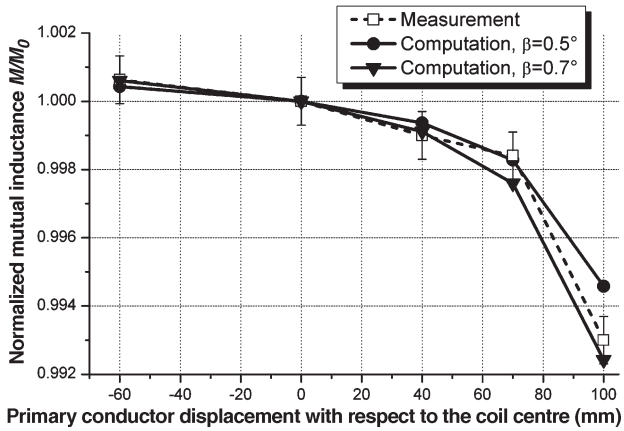

Fig. 9. Comparison of the measurement and model results versus displacements of the primary conductor from the coil center for two gap angles β.

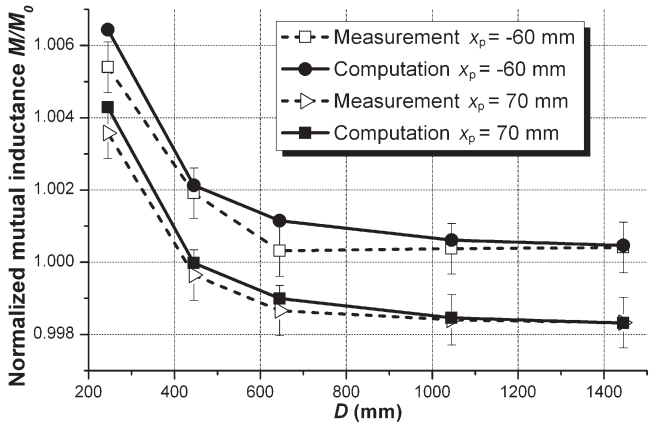

Fig. 10. Comparison of the measurement and model results as a function of the return conductor position. The displacement of the primary conductor is indicated as a parameter.

the primary conductor. The actual coil opening angle, which can only be estimated, is assumed equal to 0.5°. The maximum relative deviation between the model and the experimental results is $1.5 \cdot 10^{-3}$ when the primary conductor is very close to the gap ($x_\mathrm{p} = 100$ mm). The computation is repeated by slightly increasing the opening angle ($\beta = 0.7°$) to determine the sensitivity to the gap variation. In this case, a measurement-model deviation one order of magnitude lower is found for the same position of the primary conductor. As shown in Fig. 9, all the measurement results fall inside the strip edged by the two modeled cases.

Fig. 10 shows the influence of the return conductor distance from the coil center when the primary conductor is placed in two positions ($x_\mathrm{p} = 70$ mm, $x_\mathrm{p} = -60$ mm), with $\beta = 0.5°$.

The obtained results show an agreement between the measurement and the computation that is generally better than the

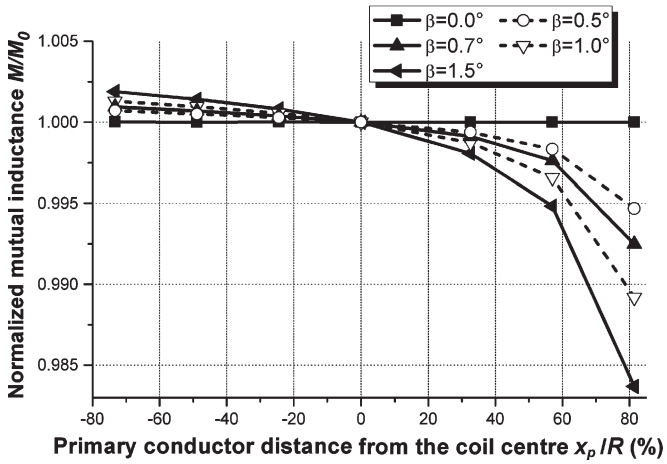

Fig. 11. Normalized mutual inductance versus primary conductor position from the coil center, for gap angles β from 0° to 1.5°.

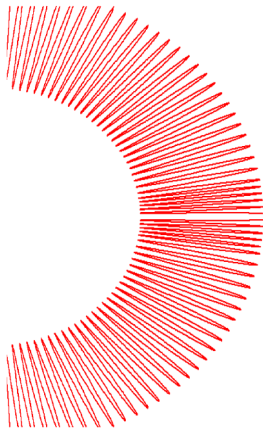

Fig. 12. Sketch of a non-uniform turn distribution along the coil.

part per thousand. The results also make feasible the use of the numerical model for an exhaustive analysis of the RC behavior.

IV. Influence of the Coil and Circuital Parameters

The analysis is carried out by simulating the RC, whose characteristics are summarized in Table II.

First, the effect of the primary conductor position on the mutual inductance is investigated by assuming angle β as a parameter.

The results are shown in Fig. 11, where the conductor is moved along the x-axis from the coil center up to 80% of the mean coil radius R. The values shown can be referred to any coil radius R.

As shown in Fig. 11, when the primary conductor is close to the coil gap, the mutual inductance decreases significantly with respect to M_0, even for small angles β. To limit this effect, the turns close to the coil terminals are concentrated by decreasing their pitch (Fig. 12). The results in Table III show that for the primary conductor position $x_\mathrm{p}/R = 0.8$, the deviation of M/M_0 from unit can be strongly lowered through a suitable choice of the number m of turns with reduced pitch (weight

TABLE III
Mutual Inductance Relative Deviation With Uniform and Non-Uniform Optimized Turn Distributions ($N = 130$)

	Uniform distribution (10^{-2})	Non-uniform distribution (10^{-2})
$\beta = 0.5°$	-0.53	0.05 (m=2)
$\beta = 0.7°$	-0.75	0.10 (m=3)
$\beta = 1.0°$	-1.08	0.03 (m=4)
$\beta = 1.5°$	-1.63	-0.10 (m=6)

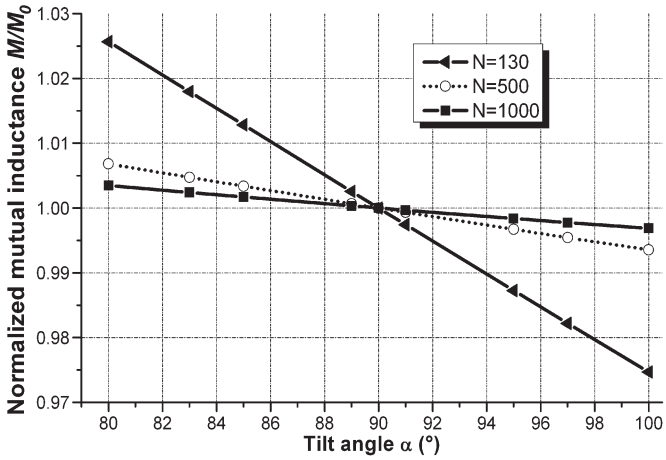

Fig. 13. Effect of non-orthogonal condition between the RC plane and the primary conductor. The mutual inductance values are shown versus angle α for increasing number N of turns ($\beta = 1°$).

$w_i = 0.9$). For larger β, m has to be increased or the weight w_i must be decreased. As an indication, an approximated rule to optimize the compensation is given by

$$\frac{2\pi}{N}\sum_{i=1}^{m}(1 - w_i) \approx \beta. \tag{5}$$

This relation is derived by imposing that the linked magnetic flux lost in the gap is compensated by the compression of the m turns. It can be noted that the results shown in Table III agree with (5).

In actual situations, the requirement of orthogonal condition between the coil plane and the primary conductor cannot always be fulfilled. For this reason, the effect of a coil tilt angle α is investigated for different values of the gap β and turn number N. In the present analysis, the primary conductor lays in the yz plane and is rotated around the x-axis (Fig. 1) in centered position. The tilt angle ranges from 80° to 100° with respect to the coil plane (orthogonal condition: $\alpha = 90°$). Fig. 13 shows and compares the deviations of the mutual inductance versus α for $\beta = 1°$, computed with 130, 500, and 1 000 turns. The results show that the behaviors are almost antisymmetric with respect to $\alpha = 90°$ and that they strongly depend on the turn number. To better understand this phenomenon, some considerations are detailed in the appendix. It must be observed that if the computation is repeated for $\beta = 0°$ (closed coil), the considered tilt α gives rise, for the considered case, to deviations that are at least one order of magnitude lower than those found with $\beta = 1°$.

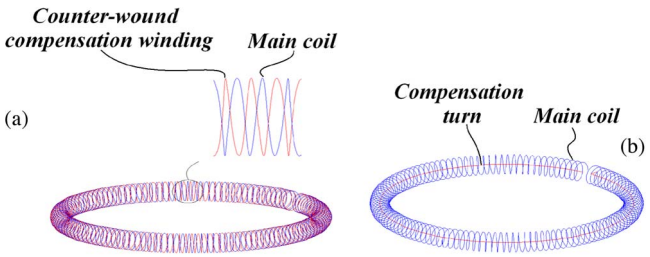

Fig. 14. Sketch of (a) a second winding counter-wound with the same turns as the main coil and (b) a counter-wound single-turn.

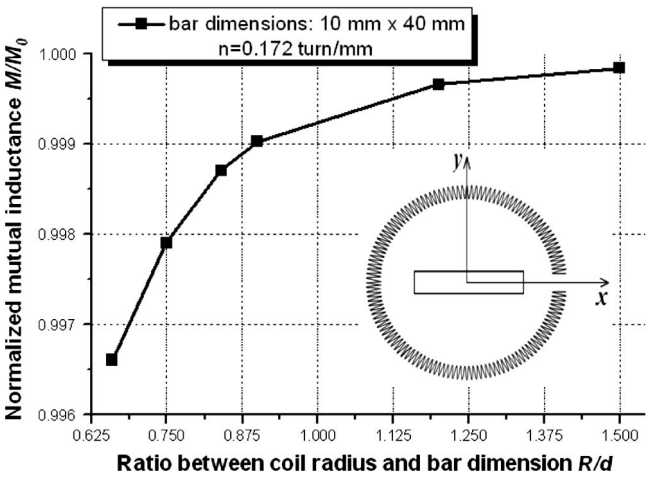

Fig. 15. Normalized mutual inductance versus the ratio of coil radius to bar dimension.

The tilt effect may be considerably reduced by adding a counter-wound winding or a counter-wound single-turn. This solution, generally adopted to mitigate possible external magnetic fields with components along the coil axis (z-axis), gives advantages also in non-orthogonal conditions. By adding a counter-wound winding with the same turn number as the main coil [Fig. 14(a)], the mutual inductance deviation reduces to less than $2 \cdot 10^{-4}$, even in the worst case ($N = 130, \alpha = 100°$). A counter-wound single-turn, instead of a second winding [Fig. 14(b)], leads to a $8 \cdot 10^{-4}$ relative deviation for the same worst case.

All the issues previously discussed concern a primary conductor of circular shape. In power plants, however, busbars are frequently used. Then, the influence on the mutual inductance of the cross-section dimensions of the primary conductor is investigated with respect to the coil radius. To this end, a rectangular conductor with dimensions $h = 10$ mm and $d = 40$ mm is centered at O with the major dimension along the x-axis. A 1-mm coil gap is assumed with a turn density $n = 0.172$ turn/mm (Fig. 15). The mutual inductance computed with the filamentary primary conductor is considered as the reference value M_0. As far as the major bar dimension is sufficiently smaller than the coil radius ($R > 1.5d$), the deviation of the mutual inductance from the reference value is negligible. If the bar conductor has the major dimension d along the y-axis, the deviation is reduced to about $6 \cdot 10^{-4}$ when $R = 0.66d$.

TABLE IV
INFLUENCE QUANTITY RANGES FOR SITUATION A

Influence quantity	Range of variation	Reference condition
Eccentricity	0.0 to 0.4	0.0
Turn pitch weight	0.95 to 1.05	1.0
Δx displacement	(-50 to +50) mm	0 mm
Δy displacement	(-30 to +30) mm	0 mm
Return conductor distance from the coil centre	(1.5 to 20)·R	20·R
Primary conductor length	(3.1 to 6) m	6 m
Tilt angle α	(70 to 110)°	90°

V. ESTIMATE OF THE ON-SITE MEASUREMENT UNCERTAINTY

When using the RC for on-site measurements, the circuit arrangement can significantly differ from the optimal one with reference to both the coil positioning around the primary conductor and the presence of the return conductor and/or other field sources. In addition, the measurement conditions strongly vary from site to site and in most cases, measurement conditions cannot be accurately determined. This situation can lead to a degradation of the RC performances since the actual value of the mutual inductance M can be different from the one determined in the reference condition (M_0). However, the high number of parameters, which cannot be well-controlled, makes direct analysis unfeasible and suggests the use of a statistical approach.

An estimate of the measurement uncertainty for an on-site situation can be performed by making use of the model previously described, starting from the identification of the influence parameters and their expected ranges of variation. In the following, examples of uncertainty evaluation are given for rough on-site measurements and better controlled measurement conditions. The flexible and openable RC, whose dimensions are listed in Table II ($\beta = 0.5°$), is fitted by a counter-wound compensation turn [Fig. 14(b)]. The influence quantities and their assumed range of variation are shown in Table IV (situation A), together with the reference condition values. The path of the primary conductor, with a circular cross-section, is divided in two parts connected in correspondence of the coil plane: the first one has a 3 m fixed length and the second section can be varied to simulate the effect of a turn made by the power circuit.

A propagation distribution approach based on the Monte Carlo method is used to estimate the mutual inductance M, its standard uncertainty, and the coverage interval corresponding to a 95% coverage probability [22]. The standard uncertainty associated with the input quantities is evaluated by assuming, as a first approach, a rectangular probability distribution of half width equal to the variation range. The number of draws T is fixed to 20 000, which is sufficient to ensure statistical stabilized results [22].

A more controlled measurement situation is taken into account by considering the reduced range of variations shown

TABLE V
INFLUENCE QUANTITY RANGES FOR SITUATION B

Influence quantity	Range of variation	Reference condition
Eccentricity	0.0 to 0.2	0.0
Turn pitch weight	0.99 to 1.01	1.0
Δx displacement	(-5 to +5) mm	0 mm
Δy displacement	(-3 to +3) mm	0 mm
Return conductor distance from the coil centre	(5 to 20)·R	20·R
Primary conductor length	(4 to 6) m	6 m
Tilt angle α	(88 to 92)°	90°

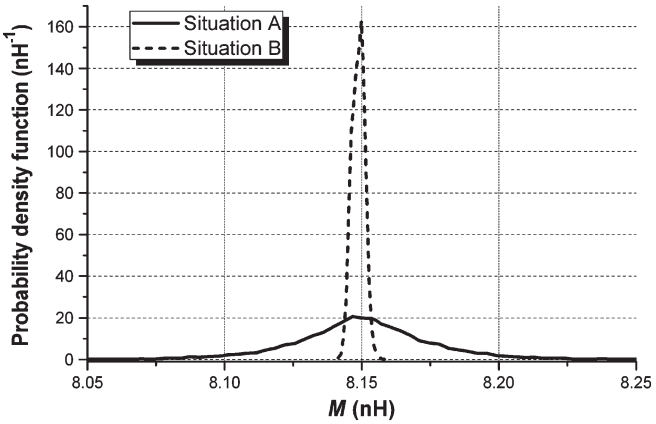

Fig. 16. Probability density functions for situations A and B.

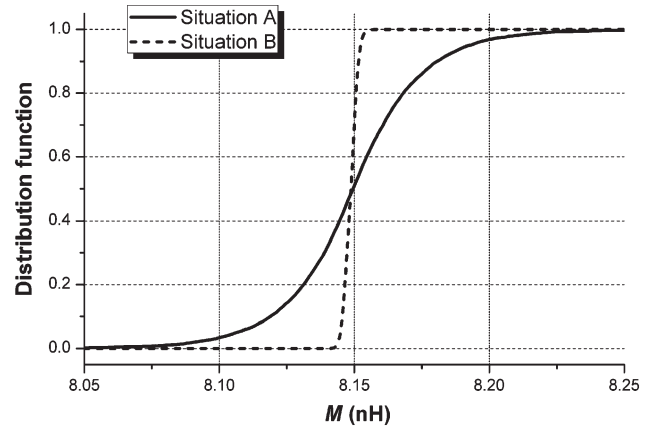

Fig. 17. Distribution functions for situations A and B.

in Table V (situation B). Figs. 16 and 17 compare the numerically approximated probability density function and distribution function for situations A and B, respectively. The difference between the estimated mutual inductances M is quite negligible ($M = 8.1503$ nH for case A and $M = 8.1487$ nH for case B, against a calculated reference value $M_0 = 8.1487$ nH). From the data shown in Fig. 16, standard deviations of 0.027 nH and 0.0023 nH are found for situations A and B, respectively. A relative standard uncertainty contribution of some parts per thousand can then be attributed to the measurement arrangement when the range of variations listed in Table IV can be reasonably assumed. However, in a relatively more controlled situation, this contribution becomes quite negligible or at most comparable with that associated to M_0, determined in the calibration phase provided that measurements are performed not too far from room temperature.

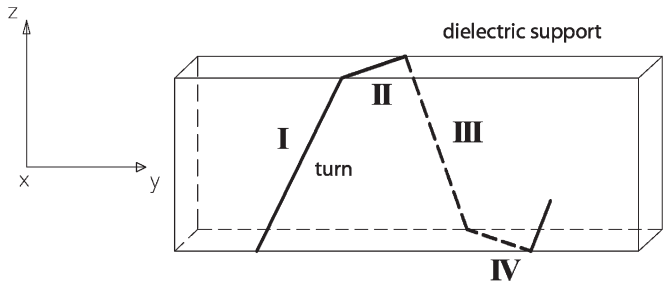

Fig. 18. Sketch of a square cross-section turn made of four straight segments (I, II, III, and IV).

VI. CONCLUSION

A modeling analysis has been developed, which is able to predict the Rogowski coil performances at power frequency when operating under non-ideal conditions. The numerical tool can be employed both in the design phase and the evaluation of the mutual inductance variation as a function of the coil structure and the power circuit arrangement. The use of the model, together with a propagation distribution approach based on the Monte Carlo method, allows an evaluation of the measurement uncertainty for those on-site arrangements where only range of variations of the influence parameters can be estimated.

According to this approach, the uncertainty associated with the use of a flexible and openable RC is finally estimated and found to be within some part per thousand in field measurement conditions.

APPENDIX

The analysis of the non-orthogonal condition effects is, in a general case, a quite complicated topic. However, under the assumption that the primary conductor is rotated around the x-axis in the plane yz (Fig. 1) and the turn number N is sufficiently high, some simplified considerations can be developed.

To this end, the RC turn opposite to the coil gap is considered. Under the assumption of a square cross-section, this turn is subdivided into four straight segments (I, II, III, and IV in Fig. 18) with length l. The contribution Λ_t to (3), related to the single turn, is expressed as

$$\Lambda_t = \int\limits_{turn} \vec{A}\cdot d\vec{\gamma} = \int\limits_{I} \vec{A}\cdot d\vec{\gamma} + \int\limits_{II} \vec{A}\cdot d\vec{\gamma} + \int\limits_{III} \vec{A}\cdot d\vec{\gamma} + \int\limits_{IV} \vec{A}\cdot d\vec{\gamma} \quad (6)$$

Fig. 19(a) and (b) show the relative orientation of the vectors involved in (6) for segments I–III and II–IV, respectively, when

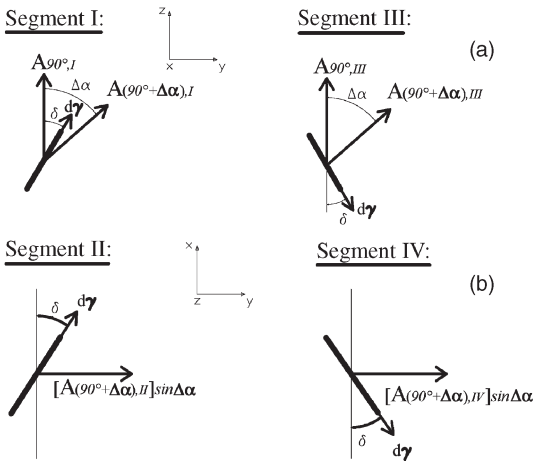

Fig. 19. Vector orientations involved in the computation of (6). (a) Segments I–III. (b) Segments II–IV.

$\alpha = 90^\circ$ and $90^\circ + \Delta\alpha\,(\Delta\alpha > 0)$. The angle δ is related to the turn pitch, which depends on the turn number N. $A_{90^\circ,i}$ and $A_{90^\circ+\Delta\alpha,i}$ are the average values of the magnetic potential along the segment i $(i = \mathrm{I}, \ldots, \mathrm{IV})$.

The flux linked with the single turn when $\alpha = 90^\circ$ is

$$\Lambda_{t,90^\circ} = \int_{turn} \vec{A}_{90^\circ} \cdot d\vec{\gamma} = A_{90^\circ,I} l \cos\delta - A_{90^\circ,III} l \cos\delta$$

$$\rightarrow \Lambda_{t,90^\circ} = l\Delta A \cos\delta \tag{7}$$

where the magnetic potentials in I and III are linked by the expression $A_{*,I} = A_{*,III} + \Delta A\ (\Delta A > 0)$. It should be noted that the integrals along II and IV are null because their paths are perpendicular to the magnetic vector potentials.

When $\alpha = 90^\circ + \Delta\alpha$, the magnetic flux becomes

$$\begin{aligned}\Lambda_{t,90^\circ+\Delta\alpha} &= \int_{turn} \vec{A}_{90^\circ+\Delta\alpha} \cdot d\vec{\gamma} \\ &= l\Big[\Delta A \cos\Delta\alpha\cos\delta + (2A_{90^\circ+\Delta\alpha,III} + \Delta A) \\ &\quad \times \sin\Delta\alpha\sin\delta + (A_{90^\circ+\Delta\alpha,II} + A_{90^\circ+\Delta\alpha,IV}) \\ &\quad \times \sin\Delta\alpha\sin\delta\Big]\end{aligned} \tag{8}$$

In a similar way, when $\alpha = 90^\circ - \Delta\alpha$ is considered, the magnetic flux is

$$\begin{aligned}\Lambda_{t,90^\circ-\Delta\alpha} &= \int_{turn} \vec{A}_{90^\circ-\Delta\alpha} \cdot d\vec{\gamma} \\ &= l\Big[\Delta A \cos\Delta\alpha\cos\delta + \\ &\quad - (2A_{90^\circ-\Delta\alpha,III} + \Delta A)\sin\Delta\alpha\sin\delta + \\ &\quad - (A_{90^\circ-\Delta\alpha,II} + A_{90^\circ-\Delta\alpha,IV})\sin\Delta\alpha\sin\delta\Big]\end{aligned} \tag{9}$$

The deviations $e_{90^\circ+\Delta\alpha} = (\Lambda_{t,90^\circ+\Delta\alpha} - \Lambda_{t,90^\circ})$ and $e_{90^\circ-\Delta\alpha} = (\Lambda_{t,90^\circ-\Delta\alpha} - \Lambda_{t,90^\circ})$ are equal to

$$\begin{aligned}e_{90^\circ+\Delta\alpha} = [&\Delta A\cos\delta(\cos\Delta\alpha - 1) + \\ &+ (2A_{90^\circ+\Delta\alpha,III} + \Delta A)\sin\Delta\alpha\sin\delta + \\ &+ (A_{90^\circ+\Delta\alpha,II} + A_{90^\circ+\Delta\alpha,IV})\sin\Delta\alpha\sin\delta]\end{aligned} \tag{10}$$

$$\begin{aligned}e_{90^\circ-\Delta\alpha} = [&\Delta A\cos\delta(\cos\Delta\alpha - 1) + \\ &- (2A_{90^\circ-\Delta\alpha,III} + \Delta A)\sin\Delta\alpha\sin\delta + \\ &- (A_{90^\circ-\Delta\alpha,II} + A_{90^\circ-\Delta\alpha,IV})\sin\Delta\alpha\sin\delta]\,.\end{aligned} \tag{11}$$

The first term of both (10) and (11) is smaller than the other ones under the above assumptions. These two relations define an antisymmetric function of the tilt angle, which can be related to the behavior of Fig. 13.

ACKNOWLEDGMENT

The authors would like to thank Dr. Domenico Giordano for his contribution to the development of the numerical model and the discussion of the results.

REFERENCES

[1] J. D. Ramboz, "Machinable Rogowski coil, design, and calibration," *IEEE Trans. Instrum. Meas.*, vol. 45, no. 2, pp. 511–515, Apr. 1996.

[2] M. Bombonato and D. D'Amore, "A classical device for the modern measurements: The Rogowski coil," "Un componente classico per le misure moderne: la bobina di Rogowski," vol. LXXVI, *L'Elettrotecnica*, no. 9, pp. 765–771, Sep. 1989.

[3] D. A. Ward, J. La, and T. Exon, "Using Rogowski coils for transient current measurements," *Eng. Sci. Educ. J.*, vol. 2, no. 3, pp. 105–113, Jun. 1993.

[4] M. Argueso, G. Robles, and J. Sanz, "Implementation of a Rogowski coil for the measurement of partial discharges," *Rev. Sci. Instrum.*, vol. 76, no. 6, pp. 065 107-1–065 107-7, Jun. 2005.

[5] L. A. Kojovic, "Rogowski coils suit relay protection and measurement," *IEEE Comput. Appl. Power*, vol. 10, no. 3, pp. 47–52, Jul. 1997.

[6] D. E. Destefan, "Calibration and testing facility for resistance welding current monitors," *IEEE Trans. Instrum. Meas.*, vol. 45, no. 2, pp. 453–456, Apr. 1996.

[7] K.-W. Lee, J.-N. Park, S.-H. Kang, Y.-S. Lee, G.-H. Ham, Y.-M. Jang, and K.-J. Lim, "Geometrical effects in the current measurement by Rogowski sensor," in *Proc. ISEIM*, Himeji, Japan, 2001, pp. 419–422.

[8] Y. Chekurov and J. Hällström, "Influence of Busbar geometry on AC current measurement using Rogowski coil," in *Proc. Dig. Precision Electromagn. Meas. Conf.*, Broomfield, CO, Jun. 8–13, 2008, pp. 542–543.

[9] K. Draxler and R. Styblikova, "Determination of Rogowski coil constant," in *Proc. Appl. Electron.*, Pilsen, Czech Republic, Sep. 2006, pp. 241–243.

[10] G. Xiaohua, L. Jingsheng, Z. Mingjun, and Y. Miaoyuan, "Improved performance Rogowski coils for power system," in *Proc. Transmiss. Distrib. Conf. Expo.*, Dallas, TX, Sep. 2003, pp. 371–374.

[11] J. D. Ramboz, D. E. Destefan, and R. S. Stant, "The verification of Rogowski coil linearity from 200 A to greater than 100 kA using ratio methods," in *Proc. IEEE Instrum. Meas. Technol.*, Anchorage, AK, May 2002, pp. 687–692.

[12] M. Faifer and R. Ottoboni, "An electronic current transformer based on Rogowski coil," in *Proc. IEEE Instrum. Meas. Technol.*, Victoria, BC, Canada, May 2008, pp. 1554–1559.

[13] J. Hlavacek, R. Prochazka, K. Draxler, and V. Kvasnicka, "The Rogowski coil design software," in *Proc. 16th IMEKO TC4 Int. Symp.*, Firenze, Italy, 2008, pp. 295–300.

[14] G. Beccherini, S. Di Fraia, M. Marracci, B. Tellini, C. Zappacosta, and G. Robles, "Critical parameters for mutual inductance between Rogowski

coil and primary conductor," in *Proc. 12MTC*, Singapore, May 2009, pp. 432–436.
[15] L. Ferkovic, D. Ilic, and R. Malaric, "Mutual inductance of a precise Rogowski coil in dependence of the position of primary conductor," *IEEE Trans. Instrum. Meas.*, vol. 58, no. 1, pp. 122–128, Jan. 2009.
[16] M. Rezaee and H. Heydari, "Mutual inductances comparison in Rogowski coil with circular and rectangular cross-sections and its improvement," in *Proc. 3rd IEEE Conf. Ind. Electron. Appl. Conf.*, Singapore, Jun. 2008, pp. 1507–1511.
[17] J. Letosa, J. S. Artal, M. Samplon, A. Uson, and F. J. Arcega, "Modelization of current sensors by finite elements method," *Measurement*, vol. 35, no. 3, pp. 233–241, Apr. 2004.
[18] G. Crotti, D. Giordano, and A. Morando, "Analysis of Rogowski coil behavior under non ideal measurement conditions," in *Proc. XIX IMEKO*, Lisbon, Portugal, Sep. 2009, pp. 876–881.
[19] Q. Chen, H. Li, M. Zhang, and Y. Liu, "Design and characteristics of two Rogowski coils based on printed circuit board," *IEEE Trans. Instrum. Meas.*, vol. 55, no. 3, pp. 939–943, Jun. 2006.
[20] C. D. M. Oates, A. J. Burnett, and C. James, "The design of high performance Rogowski coils," in *Proc. Power Electron., Mach. Drives Conf.*, Bath, U.K., Apr. 2002, pp. 568–572.
[21] O. Bottauscio, M. Chiampi, and D. Chiarabaglio, "Magnetic flux distribution and losses in narrow ferromagnetic strips," *J. Magn. Magn. Mater.*, vol. 215/216, pp. 46–48, Jun. 2000.
[22] Joint Committees for Guides in Metrology, Supplement 1 to the "Guide to the Expression of Uncertainty in Measurement"–Propagation of Distributions Using a Monte Carlo Method2008.

Mario Chiampi received the degree in electrotechnical engineering from Politecnico di Torino, Torino, Italy, in 1973.

From 1978 to 1987, he was a Research Scientist with the Istituto Elettrotecnico Nazionale Galileo Ferraris, Torino. He is currently a Full Professor of fundamentals of electrical engineering with the Dipartimento di Ingegneria Elettrica, Politecnico di Torino. His research interests include numerical methods for electromagnetics, magnetic material modeling, and computer-aided design of electrical devices.

Gabriella Crotti received the degree in physics from the University of Torino, Torino, Italy, in 1986.

Since 1987, she has been with the Electromagnetics Division, Istituto Elettrotecnico Nazionale Galileo Ferraris (now Istituto Nazionale di Ricerca Metrologica), Torino. Her research interests include the development of references and measurement techniques of high voltages, high currents, and low- and intermediate-frequency electromagnetic fields.

Andrea Morando was born in San Paolo, Brazil, in 1984. He received the B.Sc. and M.Sc. degrees in electrical engineering from the Politecnico di Torino, Torino, Italy, in 2006 and 2008, respectively, where he is currently working toward the Ph.D. degree in electrical engineering.

His research interests include the development and application of numerical methods and the experimental study for investigating electromagnetic compatibility problems and current transducers.